ACS OMEGA

Open Access

http://pubs.acs.org/journal/acsodf

Article

Impact of Surface Charge-Tailored Gold Nanorods for Selective Targeting of Mitochondria in Breast Cancer Cells Using Photodynamic Therapy

Nadar Manimaran Vinita, Umapathy Devan, Sabapathi Durgadevi, Selvaraj Anitha, Muthusamy Govarthanan, Arockiam Antony Joseph Velanganni, Jeyaraman Jeyakanthan, Pitchan Arul Prakash, Mohamed Sultan Mohamed Jaabir, and Ponnuchamy Kumar*

Cite This: *ACS Omega* 2023, 8, 33229−33241

Read Online

ACCESS | Metrics & More | Article Recommendations | Supporting Information

ABSTRACT: Herein, the impact of surface charge tailored of gold nanorods (GNRs) on breast cancer cells (MCF-7 and MDA-MB-231) upon conjugation with triphenylphosphonium (TPP) for improved photodynamic therapy (PDT) targeting mitochondria was studied. The salient features of the study are as follows: (i) positive (CTAB@GNRs) and negative (PSS-CTAB@GNRs) surface-charged gold nanorods were developed and characterized; (ii) the mitochondrial targeting efficiency of gold nanorods was improved by conjugating TPP molecules; (iii) the conjugated nanoprobes (TPP-CTAB@GNRs and TPP-PSS-CTAB@GNRs) were evaluated for PDT in the presence of photosensitizer (PS), 5-aminolevulinic acid (5-ALA) in breast cancer cells; (iv) both nanoprobes (TPP-CTAB@GNRs and TPP-PSS-CTAB@GNRs) induce apoptosis, damage DNA, generate reactive oxygen species, and decrease mitochondrial membrane potential upon 5-ALA-based PDT; and (v) 5-ALA-PDT of two nanoprobes (TPP-CTAB@GNRs and TPP-PSS-CTAB@GNRs) impact cell signaling (PI3K/AKT) pathway by upregulating proapoptotic genes and proteins. Based on the results, we confirm that the positively charged (rapid) nanoprobes are more advantageous than their negatively (slow) charged nanoprobes. However, depending on the kind and degree of cancer, both nanoprobes can serve as efficient agents for delivering anticancer therapy.

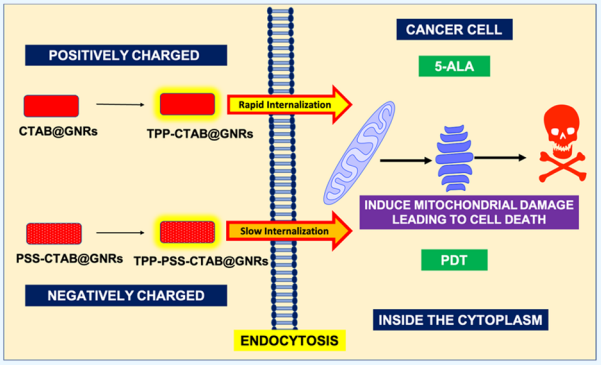

1. INTRODUCTION

On a nanoscale, gold is a versatile metal well studied for its tunable optical properties with various applications ranging from catalysis,[1] biology,[2] nonlinear optics,[3] electronics,[4] and unimaginable domains in the technology field and medicine.[5] Over the past decades, remarkable progress has been accomplished by using gold nanoparticles (GNPs).[6,7]

For example, gold nanoparticles as small molecules and drug conjugates enhance targeting with adequate release kinetics.[8−11] Moreover, the mounting evidence of nanoparticle size and surface charge determines their innate behavior in a biological system and intracellular fate.[12−15] For instance, the ability of hybrid gold nanoparticles with modified shapes to deliver doxorubicin is remarkable.[16−18] In this aspect, elongated (nanorods) and spiky (nanoprisms) gold nanoparticles are mostly appropriate for biomedical applications.[19−22]

In this journey, gold nanorods (GNRs) exert localized surface plasmon resonance (LSPR) with two absorption bands.[23,24] The most convenient method is the use of hexadecyltrimethylammonium bromide (CTAB) as a template for the growth of GNRs. Being a toxic agent, CTAB can be modified with derivatives or macromolecules that can be taken for improved biomedical applications.[25,26] Leonov et al. achieved biocompatible GNRs by detoxification with polystyrene, an anionic polyelectrolyte, for long-term stability in physiological conditions.[27]

Mirza and Shamshad fabricated doxorubicin-functionalized PSS-coated GNRs to resist CTAB.[28] In addition, Du et al. reported the highly efficient poly(ethylene glycol)-capped GNRs for photothermal ablation (PTA) of hepatocellular carcinoma.[29] Also, a plethora of reports is available on the surface modification of GNRs for improved drug delivery applications.[30−32]

Received: October 19, 2022
Accepted: March 10, 2023
Published: September 4, 2023

https://doi.org/10.1021/acsomega.2c06731
ACS Omega 2023, 8, 33229−33241

In oncology, GNPs are prominent agents that aid in the conversion of radiations into heat.[33] Taking this as an advantage, Vines et al. reviewed the role of irradiation of GNPs to ablate the tumor.[34] Similarly, the use of photosensitizer with GNRs can able to overcome drug resistance by sensitizing cancer cells.[35]

In a similar manner, photodynamic treatment (PDT) describes the dynamic interplay between light and a photosensitizer that generates molecular oxygen that selectively destroys target tissues.[36] It has been reported that several biomolecules with strong affinity for tumors can be covalently linked to the photosensitizer to boost its efficacy.[37,38]

Meanwhile, using naturally occurring amino acids, 5-aminolevulinic acid (5-ALA), is indispensable. Abo-Zeid et al. reported using 5-ALA for PDT to trigger DNA damage in breast cancer and hepatocellular carcinoma by PDT.[39] Sando et al. reported using 5-ALA-mediated targeting of aggressive adult T-cell leukemia/lymphoma resistance cells to conventional chemotherapy.[40] Meanwhile, Eskiler et al. reported the optimization of 5-ALA in PDT among various intrinsic subtypes of breast cancer cells.[41]

To assist PDT, lipophilic triphenylphosphonium cation can be delivered into cells targeting mitochondria.[42,43] TPP-functionalized nanoprobes were developed to probe mitochondrial targeting and imaging in HeLa cells.[44] Yang et al. reported the delivery of cationic TPP-functionalized GNP $^{(+/-)}$ target breast cancer cells.[45] In the above study, the positively charged GNPs are actively taken up by breast cancer cells that elevate the production of reactive oxygen species (ROS) aided by PDT treatment. Despite this, no hypotheses on the molecular mechanism by which TPP−GNRs conjugate kills cancer cells have been put forth.

Considering this, the impact of surface charge on breast cancer was studied using positively and negatively charged GNRs. These nanostructures were further conjugated with a zwitterion, thiolated triphenylphosphonium targeting mitochondrial dysfunction. To ensure photodynamic property (PDT), we then used a photosensitizer (5-ALA) along with GNRs $^{(+/-)}$ and evaluated the impact of radiation on breast cancer cells.

Altogether, gene and protein expression studies have traced the molecular mechanism involved in killing breast cancer cells. The obtained results open new avenues in choosing surface charge-impregnated gold nanorods for the selective targeting of breast cancer for potential PDT treatment.

2. MATERIALS AND METHODS

2.1. Chemicals. Chloroauric acid ($HAuCl_4 \cdot 3H_2O$), CTAB, sodium borohydride ($NaBH_4$), L-ascorbic acid, sodium chloride, sodium poly(styrene sulfonate) (PSS, M_w: 70 kDa), and methyltriphenylphosphonium bromide were purchased from Sigma-Aldrich, India. Cell culture-related media chemicals were procured from HiMedia Laboratories, India. Primers were obtained from Eurofins, India. Primary and secondary antibodies used in the study were purchased from Cell-Signaling Technologies, India. All other chemicals obtained in the study were used without any further purification.

2.2. Instrumentation. Instrumentation includes UV−visible spectrophotometer (Evolution-201, Thermo), Fourier transform infrared (FTIR) spectroscopy (Nicolet iS5, Thermo), high-resolution-transmission electron microscope (HR-TEM, Joel-2100) coupled with selected area diffraction (SAED), X-ray diffractometry (XRD, X'Pert Pro-PAnalytic, U.K.), X-ray photoelectron spectroscopy (XPS, PHI−VERSAPROBE III), energy-dispersive X-ray spectroscopy (EDS, TESCAN OXFORD), dynamic light scattering analyzer (Zetasizer Nano-Zs90, Malvern, U.K.), and inductively coupled plasma emission spectroscopy (ICPE-9800 series).

2.3. Synthesis of Gold Nanorods (GNRs). To synthesize positively charged GNRs, a modified silver-ion-assisted seed-mediated method was utilized.[20] In a 20 mL glass beaker, seed solution was prepared by swirling $HAuCl_4$ (0.01 M, 0.25 mL) and CTAB (0.05 M, 10 mL). Further, a solution with a brownish-yellow color was obtained by adding 0.6 mL of 0.01 M ice-cold $NaBH_4$ followed by 2 min of vigorous stirring. The as-formed seed solution was stored in a water bath for at least 2 h before use. In order to produce gold nanorods, growth solution was prepared by continuously stirring $HAuCl_4$ (0.01 M, 2 mL) and $AgNO_3$ (0.01 M, 0.4 mL) with CTAB (0.05 M, 40 mL). The pH of the mixture in the range between 1 and 2 was maintained using 1 M of HCl. To this mixture, L-ascorbic acid (0.1 M, 0.32 mL) was added; as a result, the solution became transparent. In the end, 0.096 mL of seed solution was added to the growth solution, stirred gently, and left undisturbed overnight at room temperature. As a result, the color of the solution deepened to ruby red, signifying the formation of GNRs with a positive charge. For the preparation of negatively charged GNRs, an anionic PSS was used. Briefly, 2 mL of positively charged GNRs (50 $\mu g\ mL^{-1}$) were allowed to react with 2 mL of anionic PSS (2 mg mL^{-1} in 6 mM NaCl) under constant stirring. The mixture was further stirred for 3 h before being centrifuged at 12,000 rpm for 10 min to remove unbound PSS, which was then resuspended in 2 mL of Milli-Q water. Both positively and negatively charged GNRs were stored at 4 °C before use. The concentration of positive and negative GNRs was determined by using the ICPE analysis.

2.4. Conjugation of Thiolated TPP. In brief, positively and negatively charged GNRs in separate reactions were added to thiolated triphenylphosphonium (TPP, 10 $\mu g/mL$) and mixed for 3 h. The unbound TPP was removed by centrifugation at 12,000 rpm for 15 min. The final product was redispersed in 2 mL of distilled water and stored at 4 °C until further use. The thiolated TPP employed in the study was prepared as described earlier.[45] UV−visible spectrophotometer assessed the TPP loading efficiency on positive and negative GNRs at 228 nm.

2.5. Cell Culture and Maintenance. Human breast cancer and normal embryonic cells were obtained from the National Centre for Cell Science in Pune and were grown as directed. Briefly, cells were grown in DMEM media supplemented with 10% FBS and 1% antibiotics (streptomycin/penicillin). The cultured cells were maintained in a humidified atmosphere with 5% CO_2 at 37 °C.

2.6. Cytotoxicity Assay. Using the MTT assay,[46] the cytotoxicity of gold probes was evaluated in human breast cancer and embryonic cells. Briefly, cells were seeded in a humid environment before attachment treatment. After attachment, the cells were treated for 24 h with a dose-dependent concentration of gold probes. Following incubation, MTT solution was added to convert the mitochondrial dehydrogenase enzyme into insoluble purple formazan crystals. DMSO was then used to dissolve the crystals, and absorbance was measured at 595 nm using a microtiter plate reader (BIORAD).

2.7. Morphological Assessment. Using several fluorescent molecular probes, the influence of the IC_{50} concentration

https://doi.org/10.1021/acsomega.2c06731
ACS Omega 2023, 8, 33229−33241

Scheme 1. Methods Involved in the Synthesis of Gold Nanorods (GNRs)

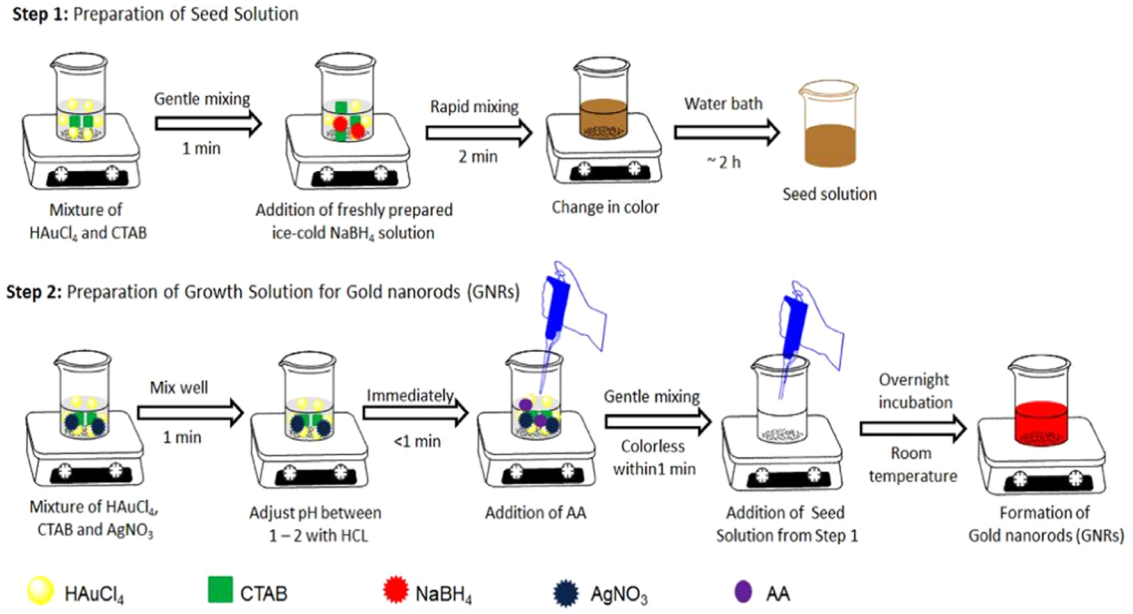

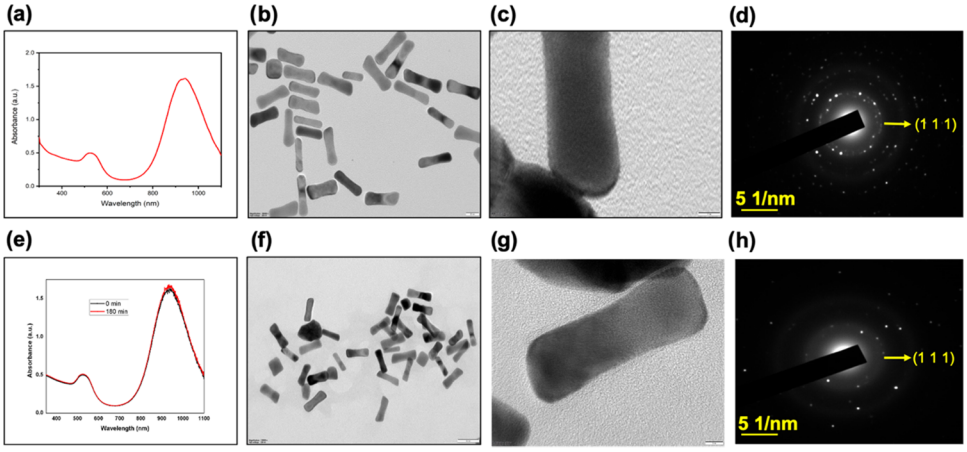

Figure 1. Optical and structural characteristics of CTAB@GNRs and PSS-CTAB@GNRs. (a) UV−vis spectroscopy of CTAB@GNRs. (b) TEM image of CTAB@GNRs (scale bar, 20 nm). (c) HR-TEM micrograph of CTAB@GNRs (scale bar, 5 nm) (d) SAED pattern of CTAB@GNRs. (e) UV−vis spectra of PSS-coated CTAB@GNRs at two intervals (0 and 180 min). (f, g) TEM and HR-TEM micrographs of PSS@CTAB@GNRs at scale bars 20 and 5 nm, respectively. (h) SAED pattern of PSS-CTAG@GNRs.

of gold probes on the morphological alterations of human breast cancer cells was investigated.[47] Dual (AO/EtBr) staining was used to examine the morphological changes that occur during apoptosis with green and red emissions. Blue-emitting Hoechst 33342 staining was employed to evaluate DNA damage in AT-rich areas. Propidium iodide staining was used to examine the DNA damage caused by red emission. DCFH-DA dye was utilized to investigate the production of reactive oxygen species in conjunction with a decrease in green intensity relative to the control (increased green emission). Finally, a green-emitting Rhodamine-123 dye examined the mitochondrial membrane potential.

2.8. Cellular PDT. As previously reported,[45] cellular PDT was performed on human breast cancer (MCF-7 and MDA-MB-231) and embryonic (HEK-293) cells in the presence of 5-aminolevulinic acid (5-ALA, 0.5 mM) and a halogen lamp was used as an irradiation source. In addition, experiments without 5-ALA and goldprobes were used with and without irradiation as control, respectively.

2.9. PpIX Formation. The intracellular PpIX formation was measured as described previously.[45] Briefly, a serum-free medium was utilized to replace human breast cancer (MCF-7 and MDA-MB-231) and embryonic (HEK-293) cells treated with IC_{50} concentration of nanoprobes, 5-ALA, or 5-ALA with nanoprobes. To evaluate PpIX kinetics, the fluorescence intensity was measured at excitation and emission wavelengths of 640 and 410 nm at different incubation times (12 and 24 h), respectively.

2.10. Cell Cycle Analysis. After PDT, the IC_{50}-treated cells were collected, washed (cold 5 mM EDTA/PBS), and resuspended in ice-cold EDTA/PBS (300 μL) and absolute ethanol (700 L). The mixture was vortexed and incubated at room temperature, followed by centrifugation at 500g for 5 min to yield a cell pellet.[48] Next, the cell pellet was redispersed in propidium iodide (100 μg/mL) and RNase (1 μg/mL) and incubated for 1 h. After incubation, the cells were subjected to flow cytometer analysis.

https://doi.org/10.1021/acsomega.2c06731
ACS Omega 2023, 8, 33229−33241

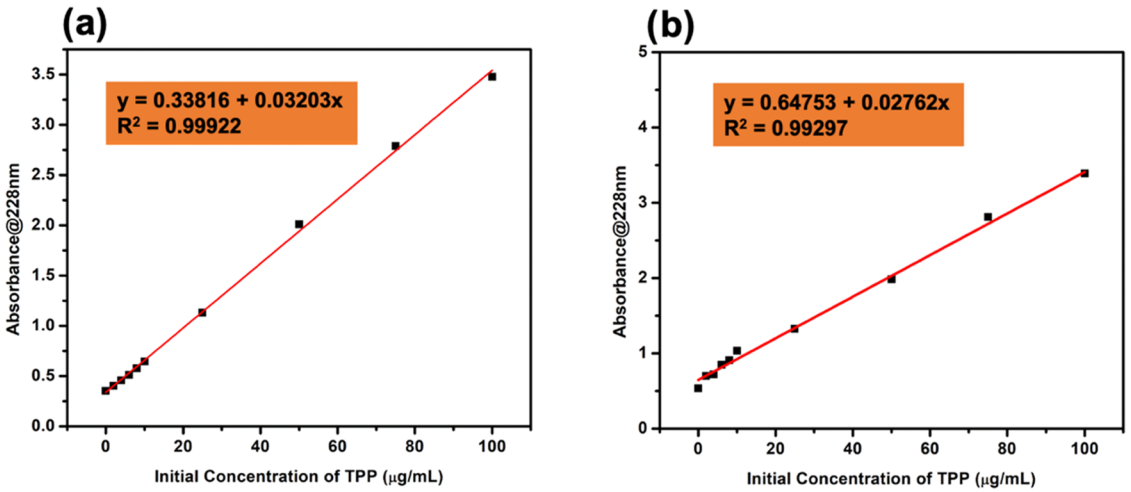

Figure 2. Increased absorbance of TPP at 228 nm after conjugation with GNRs, as shown by a linear curve. (a) TPP-CTAB@GNRs and (b) TPP-PSS-CTAB@GNRs.

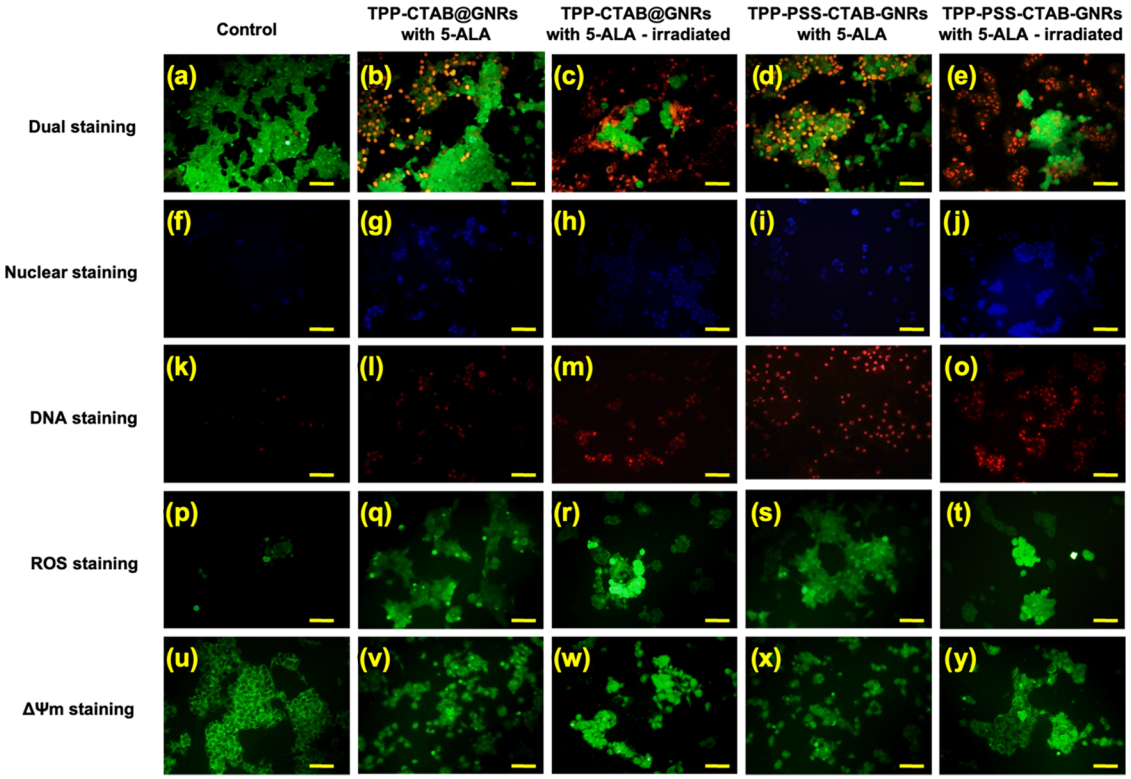

Figure 3. Images of MCF-7 breast cancer cells stained with fluorescent probes following treatment with TPP-CTAB@GNRs (IC_{50}, 0.2299 μg/mL) and TPP-PSS-CTAB@GNRs (IC_{50}, 1.012 μg/mL) in the presence of 5-ALA (0.5 mM) with and without irradiation. (a−e) Dual staining identifies live (green emission) and dead (red emission) cells stained by Acridine orange and ethidium bromide, respectively. (f−j) Nuclear staining—Hoechst 33342 binds AT-rich DNA sequences in cells whose nuclear integrity is lost and emits blue light. (k−o) DNA staining refers to the red-emitting propidium iodide used to detect DNA whose nuclear membrane permeability has been compromised. (p−t) ROS staining refers to the use of DCFH-DA, which emits green light, to identify the production of ROS within cells. (u−y) Mitochondrial membrane potential labeling employs Rhodamine-123 to demonstrate a decrease in mitochondrial membrane potential with green emission in treated cells. Scale bar: 125 μm.

2.11. Annexin V-FITC Apoptosis Assay. Cellular apoptosis in breast cancer cells upon treatment with IC_{50} concentration of gold probes in the presence of 5-ALA with irradiation was evaluated by Annexin V-FITC/PI assay kit (Invitrogen).[47] The IC_{50} treated cells were washed, trypsinized, and centrifuged to obtain a cell pellet. The cell pellet was resuspended in binding buffer, followed by the addition of Annexin V-FITC/PI. The mixture was incubated for 10 min at 25 °C and subjected to a flow cytometer.

2.12. Gene Expression Studies. After irradiation with 5-ALA, mRNA expression levels of antiapoptotic and proapoptotic genes of breast cancer cells (MCF-7 and MDA-MB-231) were evaluated by semireverse transcriptase PCR (RT-PCR) utilizing IC_{50} concentration of gold probes.[49] First, RNA was extracted using TRIzol reagent, as previously reported. Then,

https://doi.org/10.1021/acsomega.2c06731
ACS Omega 2023, 8, 33229−33241

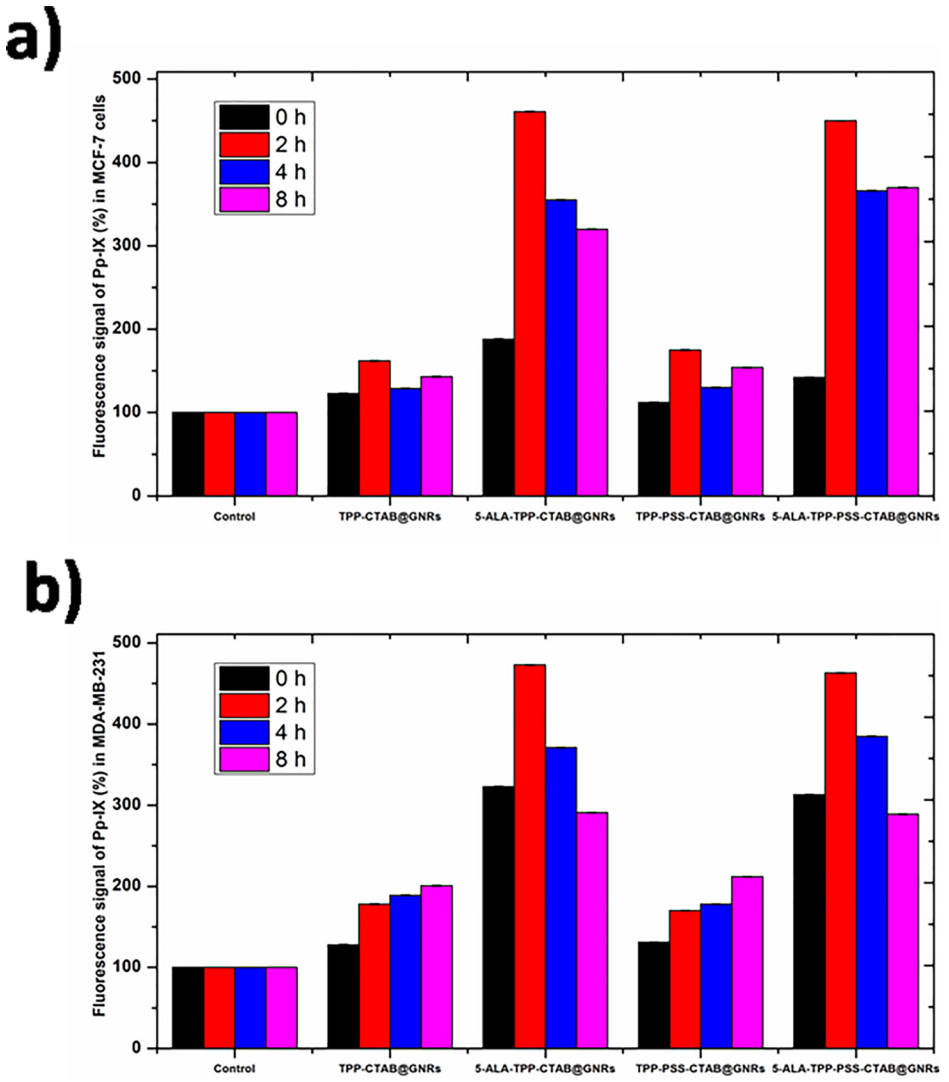

Figure 4. PpIX formation in breast cancer cells upon incubation with TPP-CTAB@GNRs and TPP-PSS-CTAB@GNRs in the presence of 0.5 mM 5-ALA with irradiation at different time intervals of incubation. (a) MCF-7 breast cancer cells and (b) MDA-MB-231 breast cancer cells.

the isolated RNA was subjected to RT-PCR using PrimeScript 1st strand cDNA Synthesis kit one-step RT-PCR (Takara, Japan). The respective gene-specific primers are tabulated in the Supporting Information (SI), Table S1. The final PCR product obtained was separated (Agarose gel), stained (ethidium bromide), and visualized (LAS 500 bioimaging system, GE). β-actin (β-actin) served as an internal control.

2.13. Western Blot Analysis. Proteins from breast cancer cells (MCF-7 and MDA-MB-231) upon treatment with IC_{50} concentration of gold probes after irradiation with 5-ALA were extracted using RIPA buffer.[47,49] The proteins isolated were quantified, and about 40 g of protein was subjected to sodium dodecyl sulfate-polyacrylamide gel electrophoresis (SDS-PAGE). Further, Western blot analyses were performed with standard procedures. Beta actin (β-actin) served as an internal control.

2.14. Statistical Analysis. All of the data in this study were obtained at least 3 times and expressed as the mean and standard deviation. Two-way ANOVA analysis with a p-value of <0.0001 (****), 0.0001 (***), 0.0025 (**), and ns (non-significant) was used to determine statistical significance.

3. RESULTS AND DISCUSSION

In recent years, gold nanorods (GNRs) have received immense attention due to their intriguing optical characteristics.[50−52] In most cases, the seed-mediated method is considered appropriate for synthesizing GNRs with more excellent stability and repeatability.[53] However, surfactant (CTAB) during the preparation of GNRs for biomedical applications is a significant constraint.[54] Taking this into account, the study's main objective is to develop GNRs at a low concentration of surfactant has shown in Scheme 1.

UV−vis spectroscopy verified the presence of longitudinal and transverse SPR bands at 901 and 524 nm, respectively (Figure 1a). CTAB capping on the surface of GNRs was confirmed by FTIR analysis, which indicated a prominent adsorption peak between 3500 and 2800 cm^{-1} for C−H stretching vibrations of methyl and methylene groups. The bands between 1500 and 1400 cm^{-1} are caused by C−H bending vibrations of CTAB (SI, Figure S1). This indicates the existence of CTAB layers on the surface of GNRs.[55] The FCC structures for gold were confirmed by X-ray diffraction analysis (SI, Figure S2). The core-level spectrum of the Au 4f doublet peaks at 82.40 and 86.01 eV for gold is authenticated by XPS

https://doi.org/10.1021/acsomega.2c06731
ACS Omega 2023, 8, 33229−33241

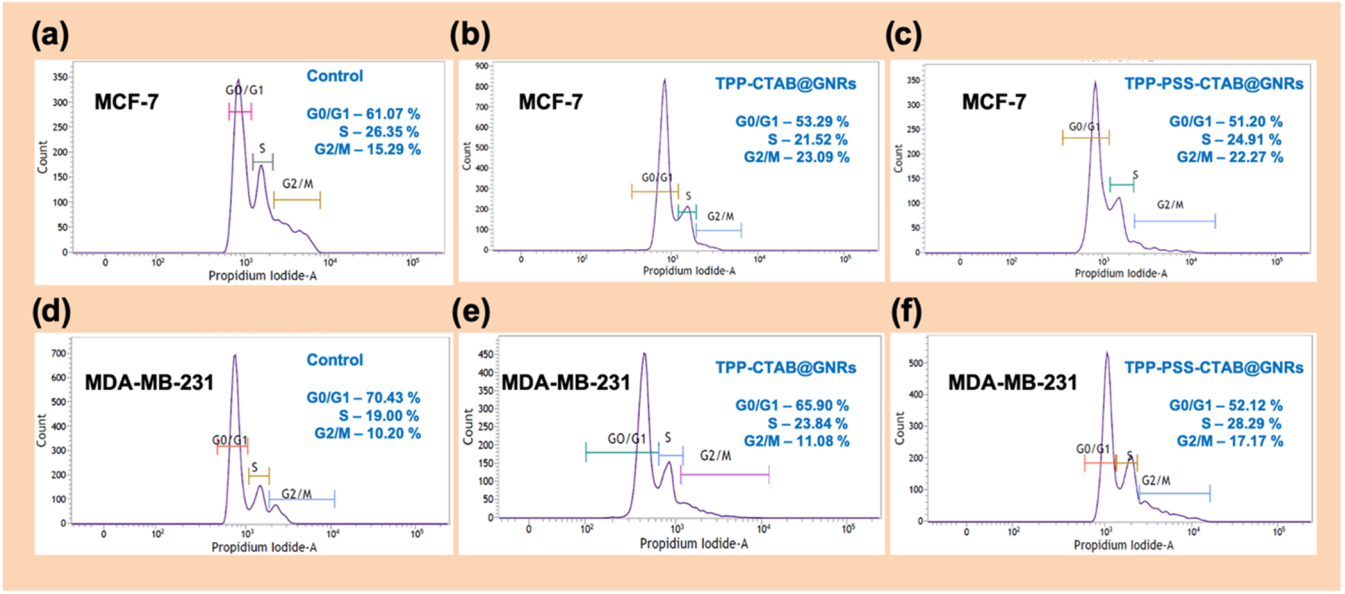

Figure 5. Cellular cycle distribution DNA analysis in MCF-7 (a−c) and MDA-MB-321 (d−f) breast cancer cells in the presence of 5-ALA (0.5 mM) with PDT. (a, d) Control (untreated) cells. (b, e) TPP-CTAB@GNRs. (c, f) TPP-PSS@CTAB@GNRs. The proliferation of cell population at different phases shows distinct peaks: G0/G1, S, and G2/M phases.

analysis (SI, Figure S3). EDS analysis confirmed the presence of metallic gold, carbon, and oxygen peaks, inferring the adsorption of CTAB on the surface GNRs (SI, Figure S4).

HR-TEM analysis confirmed the formation of CTAB@GNRs with an aspect ratio of 3.6 (Figure 1b,c). The SAED analysis confirms the diffraction pattern for FCC gold rings at (111) (Figure 1d). The hydrodynamic diameter of CTAB@GNRs was 34.34 ± 1.95 nm (SI, Figure S5). The ζ-potential measurement authenticates the existence of positively charged CTAB@GNRs with a net surface charge value of +34.1 ± 9.74 mV (SI, Figure S6). The study also inferred that the positive charge of CTAB@GNRs is attributed mainly to CTAB. Meanwhile, the CTAB bilayer remained non-covalently conjugated onto the surface of GNRs. The results from the study are concurrent with earlier reports.[20,53]

Further, the surface charge of positively charged gold nanorods was modified into a negative charge by poly(sodium 4-styrene sulfonate) (PSS).[20,56] The polyelectrolyte coating renders biocompatibility and stability to GNRs for various applications.[57,58] The excitation spectra of PSS-CTAB@GNRs showed a blue shift after the electrolyte coating (SI, Figure 1e). The FTIR analysis confirmed the existence of a sharp peak at 1500 cm^{-1}, confirming the presence of C−C stretching vibrations of PSS. In addition, the signature peaks for CTAB diminished due to PSS coating (SI, Figure S7). XRD analysis shows the existence of FCC gold at lattice planes of {111} (SI, Figure S8). Further, the XPS analysis authenticates the presence of doublet metallic gold peaks at 82.19 and 85.79 eV (SI, Figure S9).

The atomic chemical composition of PSS-CTAB@GNRs infers the existence of apparent signals for metallic gold (SI, Figure S10). A slight increase in size is noticed, inferring the coating of PSS under HR-TEM analysis (Figure 1f,g). The SAED analysis of PSS-CTAB@GNRs is concurrent with CTAB@GNRs (Figure 1h). The average size of PSS-CTAB@GNRs was 41.68 ± 1.60 nm, slightly higher than CTAB@GNRs (SI, Figure S11). This could be due to the coating of PSS onto the surface of CTAB@GNRs. The layer of polyelectrolyte (PSS) renders a negative ζ-potential value of −42.5 ± 9.89 mV (SI, Figure S12).[20] In both cases, the observed ζ-potential values were greater than ±30 mV, confirming their stability in an aqueous medium and remaining stable under special storage conditions (4 °C) for about 3 months (SI, Table S2).

The cytotoxicity of CTAB@GNRs and PSS-CTAB@GNRs was evaluated against breast cancer (MCF-7 and MDA-MB-231) and normal embryonic (HEK-293) cells by MTT assay. The as-prepared gold nanoparticles possessed improved cytotoxicity, as shown in SI, Table S3. The cytotoxicity of positively charged CTAB@GNRs is significantly higher than that of negatively charged PSS-CTAB@GNRs.[59−61] This is attributed to the capping of CTAB onto the surface of the positively charged GNRs.[20] It has also been reported that the positively charged GNRs readily transverse the negatively charged cell membranes than negative counterparts.[45,62] Furthermore, the CTAB@GNRs and PSS-CTAB@GNRs show valid signs of apoptotic cell death such as nuclear beading, chromatin condensation, generate reactive oxygen species, and disrupt mitochondria in breast cancer (MCF-7 and MDA-MB-231) cells (SI, Figures S13 and S14).[47,49]

Meanwhile, the main strategy of the study is to functionalize CTAB@GNRs and PSS-CTAB@GNRs with thiolated TPP. This was achieved by a simple stirring method followed by UV−vis spectroscopic measurement. It can be seen from the peak at 229 nm that the increasing concentration of TPP (0−300 μg/mL) represents successful functionalization upon CTAB@GNRs and PSS-CTAB@GNRs, as shown in SI, Figure S15. Meanwhile, FTIR spectroscopy of TPP is shown in SI, Figure S16a. In this process, a strong electrostatic interaction between a C−H group of CTAB and an S−H group of TPP authenticates the conjugation (SI, Figure 16b). Being a zwitterion, the TPP readily interacts with the C−C group of PSS via electrostatic (non-covalent) bonding[41,42] (SI, Figure 16c). In our study, CTAB@GNRs and PSS-CTAB@GNRs possess a net surface charge of +34.1 ± 9.74 and −42.5 ± 9.86 mV, respectively (SI, Figures S6 and S12). Meanwhile, the ζ-

https://doi.org/10.1021/acsomega.2c06731
ACS Omega 2023, 8, 33229−33241

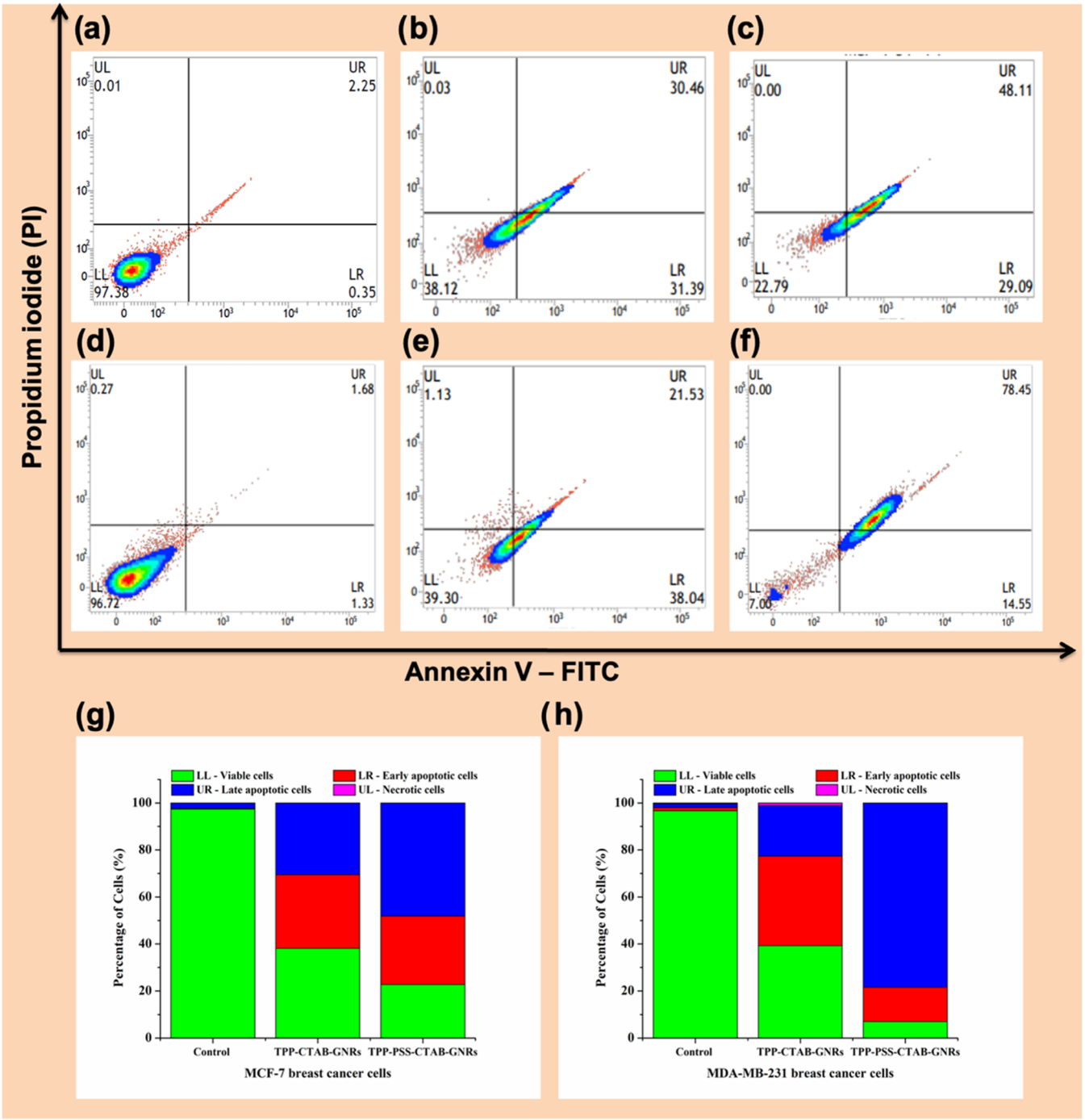

Figure 6. Annexin V-FITC/PI analysis in flow cytometry showed that 5-ALA (0.5 mM)-based PDT caused apoptotic cell death in MCF-7 (a−c) and MDA-MB-321 (d−f) breast cancer cells. (a, d) Control (untreated) cells. (b, e) TPP-CTAB@GNRs. (c, f) TPP-PSS@CTAB@GNRs. (g, h) Percentage of apoptotic cell death after PDT inferring viable and non-viable cells upon treatment with TPP-CTAB@GNRs and TPP-PSS@CTAB@GNRs. The graph shows LL, viable cells; LR, early apoptotic cells; UR, late apoptotic cells; UL, necrotic cells.

potential after functionalization with thiolated TPP showed a slight change in surface charge for TPP-CTAB@GNRs (+31.8 ± 1.25 mV) and TPP-PSS-CTAB@GNRs (−27.3 ± 3.57 mV) (SI, Figure S17). The capping of thiolated TPP with CTAB@GNRs and PSS-CTAB@GNRs showed an increased hydrodynamic diameter of 51.9 ± 2.65 and 78.5 ± 3.87 nm (SI, Figure S18). An increased absorbance of TPP at 228 nm after conjugation with GNRs is observed, as shown by a linear curve (Figure 2). Meanwhile, the loading efficiency of TPP onto the surface of CTAB@GNRs and PSS-CTAB@GNRs was found to be 98.01 and 99.37%, respectively (SI, Table S4).

As a mitochondrial-dependent agent, the use of TPP does not show intense toxicity against breast cancer (MCF-7 and MDA-MB-231) cells.[45,63] However, the functionalized entity showed better cytotoxicity than CTAB@GNRs and PSS-CTAB@GNRs against breast cancer cells, as shown in SI, Table S5. It is also noted that the cell viability of non-cancerous cells (HEK-293) was less after incubation for 24 h for TPP-CTAB@GNRs and TPP-PSS-CTAB@GNRs. Hence,

https://doi.org/10.1021/acsomega.2c06731
ACS Omega 2023, 8, 33229−33241

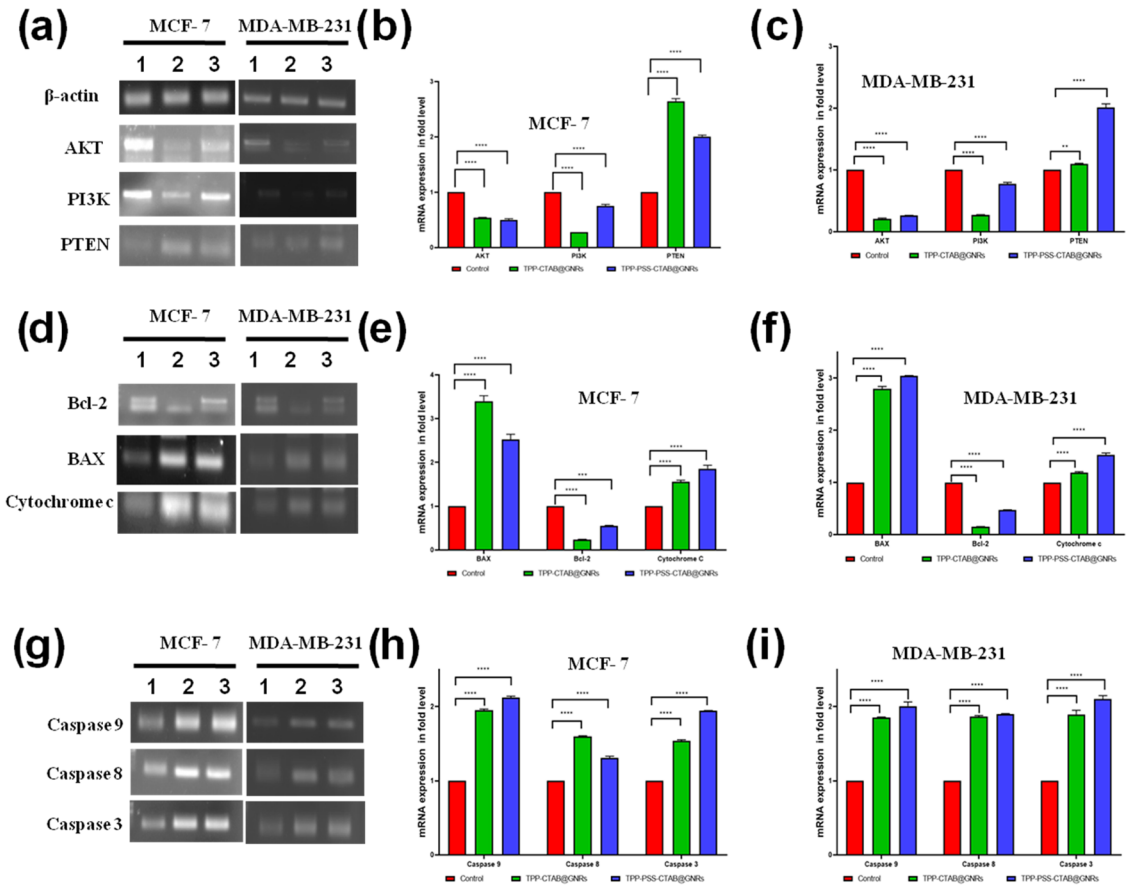

Figure 7. Involvement of pro- and antiapoptotic genes in molecular pathways of breast cancer cells treated with TPP-CTAB@GNRs and TPP-PSS@CTAB@GNRs in the presence of 0.5 mM 5-ALA followed by irradiation. (a, d, g) Gene expression pattern by semiquantitative RT-PCR for various genes in two breast cancer cells (MCF-7 and MDA-MB-231). (b, c, e, f, h, i) Fold level changes in the quantification of mRNA expression for MCF-7 and MDA-MB-321 cells. *p*-values at # <0.0001 (****), 0.0001 (***), 0.0025 (**), and ns (non-significant) were considered statistically significant. Lane 1: control (untreated cells); lane 2: TPP-CTAB@GNRs treated; lane 3: TPP-PSS@CTAB@GNRs.

it is inferred from the study that the TPP-CTAB@GNRs and TPP-PSS-CTAB@GNRs can be good candidates for biocompatibility and can be taken for further studies. In our research, the conjugated entity was also shown to cause apoptotic cell death by causing nuclear damage, increased ROS generation, and damage to mitochondria membrane potential ($\Delta\Psi m$), as demonstrated by the morphological evaluation based on fluorescence-based staining on MCF-7 (Figure 3) and MDA-MB-321 breast cancer cells (SI, Figure S19).[45,47,49]

Furthermore, the as-prepared TPP-CTAB@GNRs and TPP-PSS-CTAB@GNRs were evaluated for photodynamic effects in the presence of 5-ALA, a photosensitizer that generates singlet oxygen ($^1O_2$) in breast cancer (MCF-7 and MDA-MB-231) cells exposed to visible light. As a result of the 5-ALA treatment, an increase in cell death is noticed upon irradiation, as shown in SI, Tables S6 and S7. However, no significant difference in cell death is seen upon treatment with TPP-CTAB@GNRs and TPP-PSS-CTAB@GNRs in the presence of 5-ALA without light. The results confirmed that the accumulation of TPP-CTAB@GNRs and TPP-PSS-CTAB@GNRs in the presence of 5-ALA with light shows an improved photodynamic effect (SI, Tables S6 and S7) and further affirmed by staining in MCF-7 (Figure 3) and MDA-MB-231 (SI, Figure S19) breast cancer cells.[45,64,65] PpIX fluorescence signals were recorded based on the IC50 concentration to authenticate the above. Our study observed strong fluorescence upon irradiation with visible light compared to non-radiated TPP-CTAB@GNRs and TPP-PSS-CTAB@GNRs counterparts (Figure 4). The results obtained for PpIX fluorescence can strongly act as photosensitizers (PS) for photodynamic purposes.[40]

Besides, the effects of PDT on breast cancer cells were examined by flow cytometry analysis. The data suggest that the decrease in viable cells upon treatment with irradiated counterparts could be attributed to PDT treatment. As shown in Figure 5, a flow cytometer analysis was performed to evaluate the cell cycle arrest at distinct phases (G0/G1, G1, S, and G2/M) in breast cancer (MCF-7 and MDA-MB-231) cells treated with TPP-CTAB@GNRs and TPP-PSS-CTAB@GNRs in the presence of 5-ALA for 24 h. The cell cycle study demonstrates that TPP-CTAB@GNRs and TPP-PSS-CTAB@GNRs induced by irradiation arrest breast cancer cells in the G2/M phase.[48] As shown by fluorescence microscopy experiments, the mechanism of action is ascribed to intracellular DNA damage.[66,67] As a result, the G2 checkpoint prevents defective cells from entering mitosis and stops proliferation.

In the presence of Annexin V, the perturbation in the cellular membrane caused by the reconfiguration of phosphatidylserine (PS) on the exterior side of the cell membrane can be exploited to detect apoptosis.[68,69] As seen in Figure 6, the control cells exhibit no signs of death with normal membrane

https://doi.org/10.1021/acsomega.2c06731
ACS Omega 2023, 8, 33229−33241

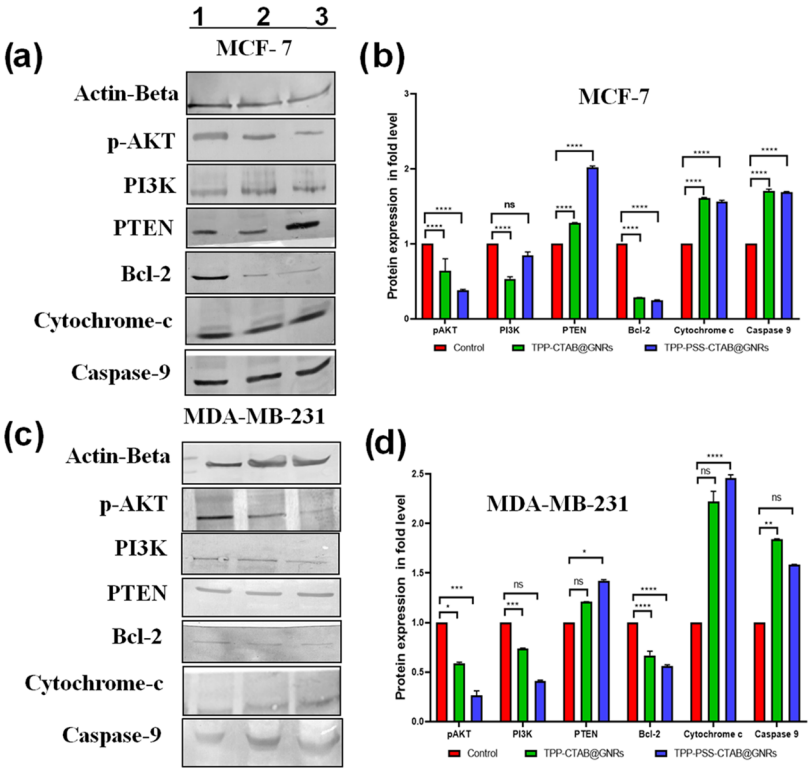

Figure 8. Western blot analysis of protein expression for pro- and antiapoptotic genes involved in molecular pathways of breast cancer cells treated with TPP-CTAB@GNRs and TPP-PSS@CTAB@GNRs in the presence of 0.5 mM 5-ALA followed by irradiation. (a, c) Protein expression pattern in two breast cancer cells (MCF-7 and MDA-MB-231). (c, d) Fold level changes in the quantification of protein expression for MCF-7 and MDA-MB-321 cells. *p*-values at # <0.0001 (****), 0.0001 (***), 0.0025 (**), 0.0015 (*), and ns (non-significant) were considered statistically significant. Lane 1: control (untreated cells); lane 2: TPP-CTAB@GNRs treated; lane 3: TPP-PSS@CTAB@GNRs.

asymmetry. However, the treatment of breast cancer (MCF-7 and MDA-MB-231) cells with TPP-CTAB@GNRs and TPP-PSS-CTAB@GNRs in the presence of 5-ALA for 24 h resulted in the externalization of phosphatidylserine (PS) during the apoptotic process, as shown by Annexin V-FITC.[70,71]

Gene and protein expression studies were conducted to investigate the involvement of the PTEN-PI3K/AKT pathway in breast cancer cells treated with TPP-CTAB@GNRs and TPP-PSS-CTAB@GNRs in the presence of 5-ALA, as shown in Figures 7 and 8.[72,73] For this purpose, IC_{50} concentrations of TPP-CTAB@GNRs and TPP-PSS-CTAB@GNRs were treated for 24 h, followed by the semiquantitative RT-PCR analysis of PTEN, PI3K, and AKT mRNA expression levels. Figure 7a–c shows the upregulation of PTEN in breast cancer cells (MCF-7 and MDA-MB-231) in the presence of TPP-CTAB@GNRs and TPP-PSS-CTAB@GNRs. In the meantime, the decreased expression levels of PI3K and AKT corroborate the inhibition of the cell survival pathway.[47,49] Furthermore, compared to untreated cancer cells, the expression pattern of p-AKT and PI3K is downregulated in both breast cancer cells (MCF-7 and MDA-MB-231), indicating the suppression of downstream kinases that regulate cellular proliferation[74] (Figure 8). In the meantime, the overexpression of PTEN dephosphorylates downstream protein targets, activating apoptosis.[75]

In addition, the gene and protein expressions of Bcl2 (antiapoptotic) and Bax (proapoptotic) in breast cancer cells treated with TPP-CTAB@GNRs and TPP-PSS-CTAB@GNRs were studied (Figures 7 and 8). The findings confirm that breast cancer cell Bcl2 expression decreased considerably after 24 h. Concurrently, the expression pattern of Bax was elevated, suggesting that this was the source of mitochondrial permeability.[76,77] In addition, the results demonstrate that a high ratio of Bax to Bcl2 can result in the release of cytochrome c, so triggering apoptosis[78,79] (Figure 7d–f). The study's findings corroborate the aforementioned claim that there was an upward trend in the gene and protein expression patterns of cytochrome c. It has also been shown that cytochrome c is released from mitochondria during the early stages of apoptosis.[80,81] Our investigation determined that the release of cytochrome c from mitochondria is a two-step mechanism that activates PTEN and Bax (Figure 8).

As cytochrome c is released from mitochondria, it interacts with Apaf-1 to form the apoptosome complex's heptameric backbone, which attracts and activates caspase-9.[82] In addition, active caspase-9 cleaves and activates caspase-3 downstream (Figure 7g–i).[47,49,83] We found that PDT with TPP-CTAB@GNRs and TPP-PSS-CTAB@GNRs induced apoptosis in breast cancer cells through the intrinsic pathway, which involves the loss of mitochondrial membrane potential. In addition to breast cancer cells being stimulated by the Fas receptor, caspase-8 was activated along with all caspases downstream (Figure 7g–i).[47,49] Based on the results, the data conclusively shows that the expression of caspase −9, −8, and −3 likely induces apoptosis in breast cancer cells (MCF-7 and MDA-MB-231) upon treatment with TPP-CTAB@GNRs and TPP-PSS-CTAB@GNRs (Figure 8), respectively.

https://doi.org/10.1021/acsomega.2c06731
ACS Omega 2023, 8, 33229−33241

4. CONCLUSIONS

In conclusion, we present the conjugation of inorganic gold nanorods (GNRs) with TPP for 5-ALA-based PDT. High cytotoxicity via endocytosis is offered by the as-prepared gold nanoprobes (TPP-CTAB@GNRs and TPP-PSS-CTAB@GNRs) in breast cancer cells (MCF-7 and MDA-MB-231). The cytotoxicity of gold nanoprobes is achieved by enhancing the production of reactive oxygen species and weakening the membrane potential of mitochondria. Overall, the gold nanoprobes as prepared suppress the cell survival (PI3K/AKT) signaling pathway that leads to apoptosis in breast cancer cells. These results demonstrate the significance of surface charge in photodynamic cancer therapy.

■ ASSOCIATED CONTENT

Supporting Information

The Supporting Information is available free of charge at https://pubs.acs.org/doi/10.1021/acsomega.2c06731.

Primers used in the study (Table S1); MTT assay (Table S2); loading efficiency of TPP onto the surface of GNRs (50 μg/mL) (Table S3); ζ-potential value of nanoprobes upon storage for up to 3 months (Table S4); MTT assay (Table S5); MTT assay with 5-ALA (Table S6); MTT assay with 5-ALA and irradiation (Table S7); FTIR spectroscopy of CTAB@GNRs (Figure S1); X-ray diffraction analysis of CTAB@GNRs (Figure S2); X-ray photoelectron spectroscopy of CTAB@GNRs (Figure S3); energy-dispersive analysis of CTAB@GNRs (Figure S4); hydrodynamic diameter (34.34 ± 1.95 nm) of CTAB@GNRs (Figure S5); surface charge by ζ-potential measurement (+34.1 ± 9.74 mV) of CTAB@GNRs (Figure S6); FTIR spectroscopy of PSS-CTAB@GNRs (Figure S7); X-ray diffraction analysis of PSS-CTAB@GNRs (Figure S8); X-ray photoelectron spectroscopy of PSS-CTAB@GNRs (Figure S9); energy-dispersive analysis of PSS-CTAB@GNRs (Figure S10); hydrodynamic diameter (41.68 ± 1.60 nm) of PSS-CTAB@GNRs (Figure S11); surface charge by ζ-potential measurement (−42.5 ± 9.89 mV) of PSS-CTAB@GNRs (Figure S12); various fluorescent staining methods were used to evaluate the nanoprobes on MCF-7 breast cancer cells to unveil the progression of apoptosis: (a−e) control (untreated) cells, (f−j) CTAB@GNRs (IC_{50}, 2.066 μg/mL), (k−o) PSS-CTAB@GNRs (IC_{50}, 5.867 μg/mL), (p−t) TPP-CTAB@GNRs (IC_{50}, 0.6096 μg/mL), and (u−y) TPP-PSS-CTAB@GNRs (IC_{50}, 1.864 μg/mL), scale bar: 125 μm (Figure S13); various fluorescent staining methods were used to evaluate the nanoprobes on MDA-MB-231 breast cancer cells to unveil the progression of apoptosis: (a−e) control (untreated) cells, (f−j) CTAB@GNRs (IC_{50}, 2.297 μg/mL), (k−o) PSS-CTAB@GNRs (IC_{50}, 7.113 μg/mL), (p−t) TPP-CTAB@GNRs (IC_{50}, 0.4732 μg/mL), and (u−y) TPP-PSS-CTAB@GNRs (IC_{50}, 0.5469 μg/mL), scale bar: 125 μm (Figure S14); conjugation of TPP (0−300 μg/mL) with GNRs (50 μg/mL): (a) CTAB@GNRs and (b) PSS-CTAB@GNRs (Figure S15); the involvement of the S−H functional group of TPP during the conjugation process with gold nanoprobes is ascertained by FTIR analysis: (a) TPP (50 μg/mL), (b) CTAB@GNRs, and (c) PSS-CTAB@GNRs (Figure S16); hydrodynamic diameter after conjugation: (a) TPP-CTAB@GNRs (51.9 ± 2.65 nm) and (b) TPP-PSS-CTAB@GNRs (78.5 ± 3.87 nm) (Figure S17); change in ζ-potential after conjugation with TPP: (a) TPP-CTAB@GNRs (+31.8 ± 1.25 mV) and (b) TPP-PSS-CTAB@GNRs (−27.3 ± 3.57) (Figure S18); and images of MDA-MB-231 breast cancer cells stained with fluorescent probes following treatment with TPP-CTAB@GNRs (IC_{50}, 0.2499 μg/mL) and TPP-PSS-CTAB@GNRs (IC_{50}, 1.114 μg/mL) in the presence of 5-ALA (0.5 mM) with and without irradiation, scale bar: 125 μm (Figure S19) (PDF)

■ AUTHOR INFORMATION

Corresponding Author

Ponnuchamy Kumar − *Food Chemistry and Molecular Cancer Biology Lab, Department of Animal Health and Management, Alagappa University, Karaikudi 630 003 Tamil Nadu, India;* orcid.org/0000-0003-1496-8840; Email: kumarp@alagappauniversity.ac.in

Authors

Nadar Manimaran Vinita − *Food Chemistry and Molecular Cancer Biology Lab, Department of Animal Health and Management, Alagappa University, Karaikudi 630 003 Tamil Nadu, India*

Umapathy Devan − *Molecular Oncology Laboratory, Department of Biochemistry, Bharathidasan University, Tiruchirappalli 620 024 Tamil Nadu, India*

Sabapathi Durgadevi − *Food Chemistry and Molecular Cancer Biology Lab, Department of Animal Health and Management, Alagappa University, Karaikudi 630 003 Tamil Nadu, India*

Selvaraj Anitha − *Food Chemistry and Molecular Cancer Biology Lab, Department of Animal Health and Management, Alagappa University, Karaikudi 630 003 Tamil Nadu, India*

Muthusamy Govarthanan − *Department of Environmental Engineering, Kyungpook National University, Deagu 41566, Republic of Korea; Department of Biomaterials, Saveetha Dental College and Hospital, Saveetha Institute of Medical and Technical Sciences, Chennai 600077 Tamil Nadu, India*

Arockiam Antony Joseph Velanganni − *Molecular Oncology Laboratory, Department of Biochemistry, Bharathidasan University, Tiruchirappalli 620 024 Tamil Nadu, India*

Jeyaraman Jeyakanthan − *Department of Bioinformatics, Alagappa University, Karaikudi 630 003 Tamil Nadu, India;* orcid.org/0000-0002-4594-9610

Pitchan Arul Prakash − *PG and Research Department of Biotechnology and Microbiology, The National College, Tiruchirappalli 620001 Tamil Nadu, India*

Mohamed Sultan Mohamed Jaabir − *PG and Research Department of Biotechnology and Microbiology, The National College, Tiruchirappalli 620001 Tamil Nadu, India*

Complete contact information is available at: https://pubs.acs.org/10.1021/acsomega.2c06731

Notes

The authors declare no competing financial interest.

https://doi.org/10.1021/acsomega.2c06731
ACS Omega 2023, 8, 33229−33241

■ ACKNOWLEDGMENTS

P.K. acknowledges the Science Engineering and Research Board (SERB), New Delhi, India, for providing financial assistance from the major research project (EEQ/2017/000135; dated: 23.03.2018). The authors also thank the support of the RUSA—Phase 2.0 grant (F. 24-51/2014U) and the University Scientific Instrumentation Centre (USIC), Alagappa University, Karaikudi, for the electron microscopic studies. Also, the authors acknowledge DST INDO-TAIWAN (GITA/DST/TWN/P-86/2019), Department of Biotechnology-Bioinformatics Centre (BIC)-No.BT/PR40154/BTIS/137/34/2021, TANSCHE (RGP/2019-20/ALU/HECP-0049 dated:27/04/2021), DST-Fund for Improvement of S&T Infrastructure in Universities & Higher Educational Institutions (FIST) (SR/FST/LSI-667/2016) (C), and DST-Promotion of University Research and Scientific Excellence (PURSE phase II) (No. SR/PURSE Phase 2/38 (G), 2017).

■ REFERENCES

(1) Ye, J.; Van Dorpe, P.; Van Roy, W.; Lodewijks, K.; De Vlaminck, I.; Maes, G.; Borghs, G. Fabrication and Optical Properties of Gold Semishells. *J. Phys. Chem. C* **2009**, *113*, 3110−3115.

(2) Si, P.; Razmi, N.; Nur, O.; Solanki, S.; Pandey, C. M.; Gupta, R. K.; Malhotra, B. D.; Willander, M.; de la Zerda, A. Gold Nanomaterials for Optical Biosensing and Bioimaging. *Nanoscale Adv.* **2021**, *3*, 2679−2698.

(3) Jagannath, G.; Eraiah, B.; Jayanthi, K.; Keshri, S. R.; Som, S.; Vinitha, G.; Pramod, A. G.; Krishnakanth, K. N.; Devarajulu, G.; Balaji, S.; Venugopal Rao, S.; Annapurna, K.; Das, S.; Allu, A. R. Influence of Gold Nanoparticles on the Nonlinear Optical and Photoluminescence Properties of Eu_2O_3 Doped Alkali Borate Glasses. *Phys. Chem. Chem. Phys.* **2020**, *22*, 2019−2032.

(4) Sousa, L. M.; Vilarinho, L. M.; Ribeiro, G. H.; Bogado, A. L.; Dinelli, L. R. An Electronic Device Based on Gold Nanoparticles and Tetraruthenated Porphyrin as an Electrochemical Sensor for Catechol. *R. Soc. Open Sci.* **2017**, *4*, No. 170675.

(5) Hu, X.; Zhang, Y.; Ding, T.; Liu, J.; Zhao, H. Multifunctional Gold Nanoparticles: A Novel Nanomaterial for Various Medical Applications and Biological Activities. *Front. Bioeng. Biotechnol.* **2020**, *8*, No. 990.

(6) Arvizo, R.; Bhattacharya, R.; Mukherjee, P. Gold Nanoparticles: Opportunities and Challenges in Nanomedicine. *Expert Opin. Drug Delivery* **2010**, *7*, 753−763.

(7) Paidari, S.; Ibrahim, S. A. Potential Application of Gold Nanoparticles in Food Packaging: A Mini Review. *Gold Bull.* **2021**, *54*, 31−36.

(8) Kuo, T.-R.; Hovhannisyan, V. A.; Chao, Y.-C.; Chao, S.-L.; Chiang, S.-J.; Lin, S.-J.; Dong, C.-Y.; Chen, C.-C. Multiple Release Kinetics of Targeted Drug from Gold Nanorod Embedded Polyelectrolyte Conjugates Induced by Near-Infrared Laser Irradiation. *J. Am. Chem. Soc.* **2010**, *132*, 14163−14171.

(9) Li, W.; Cao, Z.; Liu, R.; Liu, L.; Li, H.; Li, X.; Chen, Y.; Lu, C.; Liu, Y. AuNPs as an Important Inorganic Nanoparticle Applied in Drug Carrier Systems. *Artif. Cells, Nanomed., Biotechnol.* **2019**, *47*, 4222−4233.

(10) Zhao, Z.; Ukidve, A.; Kim, J.; Mitragotri, S. Targeting Strategies for Tissue-Specific Drug Delivery. *Cell* **2020**, *181*, 151−167.

(11) Mitchell, M. J.; Billingsley, M. M.; Haley, R. M.; Wechsler, M. E.; Peppas, N. A.; Langer, R. Engineering Precision Nanoparticles for Drug Delivery. *Nat. Rev. Drug Discovery* **2021**, *20*, 101−124.

(12) Arvizo, R. R.; Miranda, O. R.; Thompson, M. A.; Pabelick, C. M.; Bhattacharya, R.; Robertson, J. D.; Rotello, V. M.; Prakash, Y. S.; Mukherjee, P. Effect of Nanoparticle Surface Charge at the Plasma Membrane and Beyond. *Nano Lett.* **2010**, *10*, 2543−2548.

(13) Auría-Soro, C.; Nesma, T.; Juanes-Velasco, P.; Landeira-Viñuela, A.; Fidalgo-Gomez, H.; Acebes-Fernandez, V.; Gongora, R.; Parra, M. J. A.; Manzano-Roman, R.; Fuentes, M. Interactions of Nanoparticles and Biosystems: Microenvironment of Nanoparticles and Biomolecules in Nanomedicine. *Nanomaterials* **2019**, *9*, No. 1365.

(14) Di, J.; Gao, X.; Du, Y.; Zhang, H.; Gao, J.; Zheng, A. Size, Shape, Charge and "Stealthy" Surface: Carrier Properties Affect the Drug Circulation Time in Vivo. *Asian J. Pharm. Sci.* **2021**, *16*, 444−458.

(15) Jin, X.; Yu, H.; Zhang, Z.; Cui, T.; Wu, Q.; Liu, X.; Gao, J.; Zhao, X.; Shi, J.; Qu, G.; Jiang, G. Surface Charge-Dependent Mitochondrial Response to Similar Intracellular Nanoparticle Contents at Sublethal Dosages. *Part. Fibre Toxicol.* **2021**, *18*, No. 36.

(16) Wang, F.; Wang, Y.-C.; Dou, S.; Xiong, M.-H.; Sun, T.-M.; Wang, J. Doxorubicin-Tethered Responsive Gold Nanoparticles Facilitate Intracellular Drug Delivery for Overcoming Multidrug Resistance in Cancer Cells. *ACS Nano* **2011**, *5*, 3679−3692.

(17) Jang, H.; Ryoo, S.-R.; Kostarelos, K.; Han, S. W.; Min, D.-H. The Effective Nuclear Delivery of Doxorubicin from Dextran-Coated Gold Nanoparticles Larger than Nuclear Pores. *Biomaterials* **2013**, *34*, 3503−3510.

(18) Go, G.; Lee, C.-S.; Yoon, Y. M.; Lim, J. H.; Kim, T. H.; Lee, S. H. PrPC Aptamer Conjugated−Gold Nanoparticles for Targeted Delivery of Doxorubicin to Colorectal Cancer Cells. *Int. J. Mol. Sci.* **2021**, *22*, No. 1976.

(19) Dreaden, E. C.; Alkilany, A. M.; Huang, X.; Murphy, C. J.; El-Sayed, M. A. The Golden Age: Gold Nanoparticles for Biomedicine. *Chem. Soc. Rev.* **2012**, *41*, 2740−2779.

(20) Venkatesan, R.; Pichaimani, A.; Hari, K.; Balasubramanian, P. K.; Kulandaivel, J.; Premkumar, K. Doxorubicin Conjugated Gold Nanorods: A Sustained Drug Delivery Carrier for Improved Anticancer Therapy. *J. Mater. Chem. B* **2013**, *1*, 1010−1018.

(21) Gurunathan, S.; Jeyaraj, M.; La, H.; Yoo, H.; Choi, Y.; Do, J. T.; Park, C.; Kim, J.-H.; Hong, K. Anisotropic Platinum Nanoparticle-Induced Cytotoxicity, Apoptosis, Inflammatory Response, and Transcriptomic and Molecular Pathways in Human Acute Monocytic Leukemia Cells. *Int. J. Mol. Sci.* **2020**, *21*, No. 440.

(22) Costantini, P. E.; Di Giosia, M.; Ulfo, L.; Petrosino, A.; Saporetti, R.; Fimognari, C.; Pompa, P. P.; Danielli, A.; Turrini, E.; Boselli, L.; Calvaresi, M. Spiky Gold Nanoparticles for the Photothermal Eradication of Colon Cancer Cells. *Nanomaterials* **2021**, *11*, No. 1608.

(23) Li, X.; Qian, J.; Jiang, L.; He, S. Fluorescence Quenching of Quantum Dots by Gold Nanorods and Its Application to DNA Detection. *Appl. Phys. Lett.* **2009**, *94*, No. 063111.

(24) Castellana, E. T.; Gamez, R. C.; Gómez, M. E.; Russell, D. H. Longitudinal Surface Plasmon Resonance Based Gold Nanorod Biosensors for Mass Spectrometry. *Langmuir* **2010**, *26*, 6066−6070.

(25) Durr, N. J.; Larson, T.; Smith, D. K.; Korgel, B. A.; Sokolov, K.; Ben-Yakar, A. Two-Photon Luminescence Imaging of Cancer Cells Using Molecularly Targeted Gold Nanorods. *Nano Lett.* **2007**, *7*, 941−945.

(26) Wijaya, A.; Hamad-Schifferli, K. Ligand Customization and DNA Functionalization of Gold Nanorods via Round-Trip Phase Transfer Ligand Exchange. *Langmuir* **2008**, *24*, 9966−9969.

(27) Leonov, A. P.; Zheng, J.; Clogston, J. D.; Stern, S. T.; Patri, A. K.; Wei, A. Detoxification of Gold Nanorods by Treatment with Polystyrenesulfonate. *ACS Nano* **2008**, *2*, 2481−2488.

(28) Mirza, A. Z.; Shamshad, H. Fabrication and Characterization of Doxorubicin Functionalized PSS Coated Gold Nanorod. *Arabian J. Chem.* **2019**, *12*, 146−150.

(29) Du, X.; Lin, W.; Su, H. Highly Efficient Polyethylene Glycol-functionalised Gold Nanorods for Photothermal Ablation of Hepatocellular Carcinoma Cells. *IET nanobiotechnol.* **2019**, *13*, 842−849.

(30) Joshi, G.; Patel, M.; Chaudhary, D.; Sawant, K. Preparation and Surface Modification of Polymeric Nanoparticles for Drug Delivery: State of the Art. *Recent Pat. Drug Delivery Formulation* **2021**, *14*, 201−213.

(31) Khan, N. U.; Lin, J.; Younas, M. R.; Liu, X.; Shen, L. Synthesis of Gold Nanorods and Their Performance in the Field of Cancer Cell

https://doi.org/10.1021/acsomega.2c06731
ACS Omega 2023, 8, 33229−33241

Imaging and Photothermal Therapy. *Cancer Nanotechnol.* **2021**, *12*, No. 20.
(32) Osman, N.; Devnarain, N.; Omolo, C. A.; Fasiku, V.; Jaglal, Y.; Govender, T. Surface Modification of Nano-drug Delivery Systems for Enhancing Antibiotic Delivery and Activity. *WIREs Nanomed. Nanobiotechnol.* **2022**, *14*, No. e1758.
(33) Jain, S.; Hirst, D. G.; O'Sullivan, J. M. Gold Nanoparticles as Novel Agents for Cancer Therapy. *Br. J. Radiol.* **2012**, *85*, 101−113.
(34) Vines, J. B.; Yoon, J.-H.; Ryu, N.-E.; Lim, D.-J.; Park, H. Gold Nanoparticles for Photothermal Cancer Therapy. *Front. Chem.* **2019**, *7*, No. 167.
(35) Spring, B. Q.; Rizvi, I.; Xu, N.; Hasan, T. The Role of Photodynamic Therapy in Overcoming Cancer Drug Resistance. *Photochem. Photobiol. Sci.* **2015**, *14*, 1476−1491.
(36) Lee, C.-N.; Hsu, R.; Chen, H.; Wong, T.-W. Daylight Photodynamic Therapy: An Update. *Molecules* **2020**, *25*, No. 5195.
(37) Abrahamse, H.; Hamblin, M. R. New Photosensitizers for Photodynamic Therapy. *Biochem. J.* **2016**, *473*, 347−364.
(38) Calavia, P. G.; Bruce, G.; Pérez-García, L.; Russell, D. A. Photosensitiser-Gold Nanoparticle Conjugates for Photodynamic Therapy of Cancer. *Photochem. Photobiol. Sci.* **2018**, *17*, 1534−1552.
(39) Abo-Zeid, M. A. M.; Abo-Elfadl, M. T.; Mostafa, S. M. Photodynamic Therapy Using 5-Aminolevulinic Acid Triggered DNA Damage of Adenocarcinoma Breast Cancer and Hepatocellular Carcinoma Cell Lines. *Photodiagn. Photodyn. Ther.* **2018**, *21*, 351−356.
(40) Sando, Y.; Matsuoka, K.; Sumii, Y.; Kondo, T.; Ikegawa, S.; Sugiura, H.; Nakamura, M.; Iwamoto, M.; Meguri, Y.; Asada, N.; Ennishi, D.; Nishimori, H.; Fujii, K.; Fujii, N.; Utsunomiya, A.; Oka, T.; Maeda, Y. 5-Aminolevulinic Acid-Mediated Photodynamic Therapy Can Target Aggressive Adult T Cell Leukemia/Lymphoma Resistant to Conventional Chemotherapy. *Sci. Rep.* **2020**, *10*, No. 17237.
(41) Eskiler, G. G.; Ozkan, A. D.; Kucukkara, E. S.; Kamanlı, A. F.; Gunoğlu, B.; Yıldız, M. Z. Optimization of 5-Aminolevulinic Acid-Based Photodynamic Therapy Protocol for Breast Cancer Cells. *Photodiagn. Photodyn. Ther.* **2020**, *31*, No. 101854.
(42) Ross, M. F.; Kelso, G. F.; Blaikie, F. H.; James, A. M.; Cochemé, H. M.; Filipovska, A.; Da Ros, T.; Hurd, T. R.; Smith, R. A. J.; Murphy, M. P. Lipophilic Triphenylphosphonium Cations as Tools in Mitochondrial Bioenergetics and Free Radical Biology. *Biochemistry* **2005**, *70*, 222−230.
(43) Prag, H. A.; Kula-Alwar, D.; Pala, L.; Caldwell, S. T.; Beach, T. E.; James, A. M.; Saeb-Parsy, K.; Krieg, T.; Hartley, R. C.; Murphy, M. P. Selective Delivery of Dicarboxylates to Mitochondria by Conjugation to a Lipophilic Cation via a Cleavable Linker. *Mol. Pharmaceutics* **2020**, *17*, 3526−3540.
(44) Chakraborty, A.; Jana, N. R. Design and Synthesis of Triphenylphosphonium Functionalized Nanoparticle Probe for Mitochondria Targeting and Imaging. *J. Phys. Chem. C* **2015**, *119*, 2888−2895.
(45) Yang, Y.; Gao, N.; Hu, Y.; Jia, C.; Chou, T.; Du, H.; Wang, H. Gold Nanoparticle-Enhanced Photodynamic Therapy: Effects of Surface Charge and Mitochondrial Targeting. *Ther. Delivery* **2015**, *6*, 307−321.
(46) Mosmann, T. Rapid Colorimetric Assay for Cellular Growth and Survival: Application to Proliferation and Cytotoxicity Assays. *J. Immunol. Methods* **1983**, *65*, 55−63.
(47) Patel, P.; Nadar, V. M.; Umapathy, D.; Manivannan, S.; Venkatesan, R.; Joseph Arokiyam, V. A.; Pappu, S.; Prakash, P. A.; Mohamed Jabir, M. S.; Gulyás, B.; Padmanabhan, P.; Selvan, S. T.; Kumar, P. Doxorubicin-Conjugated Platinum Theranostic Nanoparticles Induce Apoptosis *via* Inhibition of a Cell Survival (PI3K/AKT) Signaling Pathway in Human Breast Cancer Cells. *ACS Appl. Nano Mater.* **2021**, *4*, 198−210.
(48) Abdel-Ghany, S.; Mahfouz, M.; Ashraf, N.; Sabit, H.; Cevik, E.; El-Zawahri, M. Gold Nanoparticles Induce G2/M Cell Cycle Arrest and Enhance the Expression of E-Cadherin in Breast Cancer Cells. *Inorg. Nano-Met. Chem.* **2020**, *50*, 926−932.
(49) Patel, P.; Umapathy, D.; Manivannan, S.; Nadar, V. M.; Venkatesan, R.; Arokiyam, V. A. J.; Pappu, S.; Ponnuchamy, K. A Doxorubicin−Platinum Conjugate System: Impacts on PI3K/AKT Actuation and Apoptosis in Breast Cancer Cells. *RSC Adv.* **2021**, *11*, 4818−4828.
(50) Grabinski, C.; Schaeublin, N.; Wijaya, A.; D'Couto, H.; Baxamusa, S. H.; Hamad-Schifferli, K.; Hussain, S. M. Effect of Gold Nanorod Surface Chemistry on Cellular Response. *ACS Nano* **2011**, *5*, 2870−2879.
(51) Wang, L.; Jiang, X.; Ji, Y.; Bai, R.; Zhao, Y.; Wu, X.; Chen, C. Surface Chemistry of Gold Nanorods: Origin of Cell Membrane Damage and Cytotoxicity. *Nanoscale* **2013**, *5*, No. 8384.
(52) Burrows, N. D.; Lin, W.; Hinman, J. G.; Dennison, J. M.; Vartanian, A. M.; Abadeer, N. S.; Grzincic, E. M.; Jacob, L. M.; Li, J.; Murphy, C. J. Surface Chemistry of Gold Nanorods. *Langmuir* **2016**, *32*, 9905−9921.
(53) Wei, M.-Z.; Deng, T.-S.; Zhang, Q.; Cheng, Z.; Li, S. Seed-Mediated Synthesis of Gold Nanorods at Low Concentrations of CTAB. *ACS Omega* **2021**, *6*, 9188−9195.
(54) Jia, Y. P.; Shi, K.; Liao, J. F.; Peng, J. R.; Hao, Y.; Qu, Y.; Chen, L. J.; Liu, L.; Yuan, X.; Qian, Z. Y.; Wei, X. W. Effects of Cetyltrimethylammonium Bromide on the Toxicity of Gold Nanorods Both In Vitro and In Vivo: Molecular Origin of Cytotoxicity and Inflammation. *Small Methods* **2020**, *4*, No. 1900799.
(55) Su, G.; Yang, C.; Zhu, J.-J. Fabrication of Gold Nanorods with Tunable Longitudinal Surface Plasmon Resonance Peaks by Reductive Dopamine. *Langmuir* **2015**, *31*, 817−823.
(56) Alex, S. A.; Chandrasekaran, N.; Mukherjee, A. Effect of Negative Functionalisation of Gold Nanorods on Conformation and Activity of Human Serum Albumin. *IET Nanobiotechnol.* **2019**, *13*, 522−529.
(57) Alkilany, A. M.; Thompson, L. B.; Murphy, C. J. Polyelectrolyte Coating Provides a Facile Route to Suspend Gold Nanorods in Polar Organic Solvents and Hydrophobic Polymers. *ACS Appl. Mater. Interfaces* **2010**, *2*, 3417−3421.
(58) Pissuwan, D.; Niidome, T. Polyelectrolyte-Coated Gold Nanorods and Their Biomedical Applications. *Nanoscale* **2015**, *7*, 59−65.
(59) Schaeublin, N. M.; Braydich-Stolle, L. K.; Schrand, A. M.; Miller, J. M.; Hutchison, J.; Schlager, J. J.; Hussain, S. M. Surface Charge of Gold Nanoparticles Mediates Mechanism of Toxicity. *Nanoscale* **2011**, *3*, No. 410.
(60) Wan, J.; Wang, J.-H.; Liu, T.; Xie, Z.; Yu, X.-F.; Li, W. Surface Chemistry but Not Aspect Ratio Mediates the Biological Toxicity of Gold Nanorods in Vitro and in Vivo. *Sci. Rep.* **2015**, *5*, No. 11398.
(61) De Berardis, B.; Marchetti, M.; Risuglia, A.; Ietto, F.; Fanizza, C.; Superti, F. Exposure to Airborne Gold Nanoparticles: A Review of Current Toxicological Data on the Respiratory Tract. *J. Nanopart. Res.* **2020**, *22*, No. 235.
(62) Fröhlich, E. The Role of Surface Charge in Cellular Uptake and Cytotoxicity of Medical Nanoparticles. *Int. J. Nanomed.* **2012**, 5577−5591.
(63) Song, H.; Xing, W.; Shi, X.; Zhang, T.; Lou, H.; Fan, P. Antitumor and Toxicity Study of Mitochondria-Targeted Triptolide Derivatives Using Triphenylphosphine (TPP+) as a Carrier. *Bioorg. Med. Chem.* **2021**, *50*, No. 116466.
(64) Shi, L.; Liu, P.; Liu, J.; Yang, Y.; Chen, Q.; Zhang, Y.; Zhang, H.; Wang, X. Application of 5-aminolevulinic Acid-photodynamic Therapy in Common Skin Diseases. *Transl. Biophotonics* **2020**, *2*, No. e201900028.
(65) Mahmoudi, K.; Garvey, K. L.; Bouras, A.; Cramer, G.; Stepp, H.; Jesu Raj, J. G.; Bozec, D.; Busch, T. M.; Hadjipanayis, C. G. 5-Aminolevulinic Acid Photodynamic Therapy for the Treatment of High-Grade Gliomas. *J. Neuro-Oncol.* **2019**, *141*, 595−607.
(66) Kang, B.; Mackey, M. A.; El-Sayed, M. A. Nuclear Targeting of Gold Nanoparticles in Cancer Cells Induces DNA Damage, Causing Cytokinesis Arrest and Apoptosis. *J. Am. Chem. Soc.* **2010**, *132*, 1517−1519.

https://doi.org/10.1021/acsomega.2c06731
ACS Omega 2023, 8, 33229−33241

(67) Ho, D.; Kretzmann, J. A.; Norret, M.; Toshniwal, P.; Veder, J.-P.; Jiang, H.; Guagliardo, P.; Munshi, A. M.; Chawla, R.; Evans, C. W.; Clemons, T. D.; Nguyen, M.; Kretzmann, A. L.; Blythe, A. J.; Saunders, M.; Archer, M.; Fitzgerald, M.; Keelan, J. A.; Bond, C. S.; Kilburn, M. R.; Hurley, L. H.; Smith, N. M.; Iyer, K. S. Intracellular Speciation of Gold Nanorods Alters the Conformational Dynamics of Genomic DNA. *Nat. Nanotechnol.* **2018**, *13*, 1148−1153.
(68) Leventis, P. A.; Grinstein, S. The Distribution and Function of Phosphatidylserine in Cellular Membranes. *Annu. Rev. Biophys.* **2010**, *39*, 407−427.
(69) Nagata, S.; Suzuki, J.; Segawa, K.; Fujii, T. Exposure of Phosphatidylserine on the Cell Surface. *Cell Death Differ.* **2016**, *23*, 952−961.
(70) Zhao, M.-X.; Cai, Z.-C.; Zhu, B.-J.; Zhang, Z.-Q. The Apoptosis Effect on Liver Cancer Cells of Gold Nanoparticles Modified with Lithocholic Acid. *Nanoscale Res. Lett.* **2018**, *13*, No. 304.
(71) Radaic, A.; Joo, N. E.; Jeong, S.-H.; Yoo, S.-I.; Kotov, N.; Kapila, Y. L. Phosphatidylserine-Gold Nanoparticles (PS-AuNP) Induce Prostate and Breast Cancer Cell Apoptosis. *Pharmaceutics* **2021**, *13*, No. 1094.
(72) Paplomata, E.; O'Regan, R. The PI3K/AKT/MTOR Pathway in Breast Cancer: Targets, Trials and Biomarkers. *Ther. Adv. Med. Oncol.* **2014**, *6*, 154−166.
(73) Azab, S.; Al-Hendy, A. Signal Transduction Pathways in Breast Cancer − Drug Targets and Challenges. In *Breast Cancer - Carcinogenesis, Cell Growth and Signalling Pathways*; Gunduz, M., Ed.; InTech, 2011.
(74) Xu, W.; Yang, Z.; Lu, N. A New Role for the PI3K/Akt Signaling Pathway in the Epithelial-Mesenchymal Transition. *Cell Adhes. Migr.* **2015**, *9*, 317−324.
(75) Lu, X.-X.; Cao, L.-Y.; Chen, X.; Xiao, J.; Zou, Y.; Chen, Q. *PTEN* Inhibits Cell Proliferation, Promotes Cell Apoptosis, and Induces Cell Cycle Arrest via Downregulating the PI3K/AKT/*HTERT* Pathway in Lung Adenocarcinoma A549 Cells. *BioMed Res. Int.* **2016**, *2016*, No. 2476842.
(76) Karch, J.; Kwong, J. Q.; Burr, A. R.; Sargent, M. A.; Elrod, J. W.; Peixoto, P. M.; Martinez-Caballero, S.; Osinska, H.; Cheng, E. H.-Y.; Robbins, J.; Kinnally, K. W.; Molkentin, J. D. Bax and Bak Function as the Outer Membrane Component of the Mitochondrial Permeability Pore in Regulating Necrotic Cell Death in Mice. *eLife* **2013**, *2*, No. e00772.
(77) Patel, P.; Mendoza, A.; Robichaux, D. J.; Wang, M. C.; Wehrens, X. H. T.; Karch, J. Inhibition of the Anti-Apoptotic Bcl-2 Family by BH3 Mimetics Sensitize the Mitochondrial Permeability Transition Pore Through Bax and Bak. *Front. Cell Dev. Biol.* **2021**, *9*, No. 765973.
(78) Kale, J.; Osterlund, E. J.; Andrews, D. W. BCL-2 Family Proteins: Changing Partners in the Dance towards Death. *Cell Death Differ.* **2018**, *25*, 65−80.
(79) Peña-Blanco, A.; García-Sáez, A. J. Bax, Bak and beyond — Mitochondrial Performance in Apoptosis. *FEBS J.* **2018**, *285*, 416−431.
(80) Eleftheriadis, T.; Pissas, G.; Liakopoulos, V.; Stefanidis, I. Cytochrome c as a Potentially Clinical Useful Marker of Mitochondrial and Cellular Damage. *Front. Immunol.* **2016**, *7*, No. 279.
(81) Ott, M.; Robertson, J. D.; Gogvadze, V.; Zhivotovsky, B.; Orrenius, S. Cytochrome *c* Release from Mitochondria Proceeds by a Two-Step Process. *Proc. Natl. Acad. Sci. U.S.A.* **2002**, *99*, 1259−1263.
(82) Cain, K. Chemical-Induced Apoptosis: Formation of the Apaf-1 Apoptosome. *Drug Metab. Rev.* **2003**, *35*, 337−363.
(83) Kumar, P.; Senthamilselvi, S.; Govindaraju, M.; Sankar, R. Unraveling the Caspase-Mediated Mechanism for Phloroglucinol-Encapsulated Starch Biopolymer against the Breast Cancer Cell Line MDA-MB-231. *RSC Adv.* **2014**, *4*, 46157−46163.

https://doi.org/10.1021/acsomega.2c06731
ACS Omega 2023, 8, 33229−33241